Electronic materials

CrossMark

Characterization and performance of porous photocatalytic ceramic membranes coated with TiO$_2$ via different dip-coating routes

Siti Salwa Alias[1], Zawati Harun[1,2,*] (iD), and Intan Suyana Abd Latif[1,2]

[1] *Advanced Manufacturing and Materials Centre (AMMC), Institute of Intergrated Engineering, Universiti Tun Hussein Onn Malaysia, 86400 Parit Raja, Johor, Malaysia*

[2] *Department of Materials and Design Engineering, Faculty of Mechanical and Manufacturing Engineering, Universiti Tun Hussein Onn Malaysia, 86400 Parit Raja, Johor, Malaysia*

ABSTRACT

Porous photocatalytic ceramic membranes have been extensively used for separation and purification processes. This study investigates the characterization and performance of porous ceramic membranes coated with TiO$_2$. The flat sheet membranes were prepared via phase inversion. The membranes were dip-coated in different concentrations of TiO$_2$ nanoparticle suspensions (0.01, 0.03 and 0.05 wt%) before sintering or after the sintering process. The ceramic membranes coated with 0.03 wt% TiO$_2$ before sintering at showed excellent morphology with a porous top, dense bottom, and the cross section showed strong adhesion of the penetrated TiO$_2$-coated layer on the surface and within the pores. This membrane exhibited the lowest surface roughness (0.05 μm) and optimum physical properties, permeation of pure water flux (128.28 L m^{-2}h^{-1}), rejection rate (86.06%), better antifouling (highest normalized flux ratio) and self-cleaning performance through increased humic acid rejection flux (94.32 L m^{-2}h^{-1}) and rejection rate (98.56%) subsequent to exposure to UV light. All of the membranes coated with different concentrations of TiO$_2$ prior to the sintering process showed uniform, homogenous coating with enhanced properties and performance. This can be related to the good penetration of TiO$_2$ nanoparticles and better absorption by the membrane structure. The accumulation of closely tied TiO$_2$ nanoparticle suspension on the surface of membranes coated after sintering has essentially blocked the membrane surface and pores which might concurrently explained their reduced performance.

Address correspondence to E-mail: zawati@uthm.edu.my

Introduction

Recently, many researchers have attempted to improve membrane separation for wastewater treatment by making use of ceramics due to its inertness which makes it impervious to various chemicals, bacteria or high temperatures [1, 2]. The common polymer membranes can be replaced with porous ceramic membranes to separate water in the purification process. These can be coated with self-cleaning inorganic photocatalytic additives (i.e., TiO_2, ZnO, CeO_2, ZrO_2, WO_3, V_2O_5, Fe_2O_3, etc.), whereas the typical polymer membranes are affected by UV irradiation [3–5]. Selecting porous ceramic membranes to treat wastewater was also due to their fouling performance at which their self-cleaning characteristic offers an excellent problem solution for deposited foulant (humic acid, HA). This is removed (or reduced) from the ceramic membrane surface via naturally occurring photocatalytic reaction. Among the self-cleaning photocatalytic materials, TiO_2 has been extensively used to solve membrane fouling due to the variations of its properties: photostability in absorbing ultraviolet (UV) light with a large bandgap (3.2 eV), high photocatalytic activity, relatively high chemical stability, low operating temperature and energy consumption, as well as water insolubility in most environmental conditions. Additionally, it also prevents the formation of undesirable by-products [6]. Dip coating is one of the most straightforward TiO_2 coating techniques that can be implemented in large-scale production. Through this method, the top surface of a porous membrane is dipped into a TiO_2 slurry suspension. The deposition of the TiO_2 coating occurs by capillary force and surface tension [7]. Although dip coating is a well-known technique, it can be further improved and the development of this technique can be further explored particularly in regard to the route of coating, temperature, duration and control of the actual condition or state of the TiO_2 suspension.

An early study by Syafei et al. [8] found that TiO_2-coated membranes did not perform any better in removing natural organic matter or reducing membrane fouling under UV irradiation. The membranes were able to remove a significant amount of humic material; however, the incorporated photocatalysis of TiO_2 has resulted in poor permeation water flux (PWF) performance. In addition to that, the TiO_2-coated membrane was not sintered at high temperature (> 1000 °C). Moreover, Zhang et al. [5] had successfully obtained a uniform TiO_2 cover of the entire surface of a hollow-fiber ceramic membrane by using a simple dip-coating technique. This technique resulted in high porosity (80%), PWF of $1700\ L\ m^{-2}h^{-1}$ and high HA removal (90%). However, this study was limited in a way that the duration of coating was not varied, and the membranes were only coated after being sintered. Nair and Jagadeesh Babu [4] claimed that integrating thin-layer TiO_2 nanosheets with graphene oxide modifiers on top of the hierarchical membrane can improve its photocatalytic activity. This is because of the stable film formation and support offered by the interconnecting TiO_2 nanosheets, in contrast to non-flexible nanoparticles. However, the PWF ($29.3\ L\ m^{-2}h^{-1}$) was low and unnecessary for a prolonged filtration process.

To the best of our knowledge, there is no preceding study that has specifically explored the varying method of coating TiO_2 nanoparticles on porous ceramic membranes, either coating before sintering or after the sintering process. Thus, this study aimed to dip-coat the porous ceramic membranes in different concentrations of TiO_2 nanoparticle suspensions before and after the membranes were sintered, characterizing the coated membranes in terms of morphology, surface roughness, diameter and thickness shrinkage, porosity, mean pore radius, water absorption, density, permeation of pure water flux (PWF) and HA rejection rate as well as evaluating the performance of the porous ceramic membranes based on a fouling test including the changing of membrane surface and HA rejection flux/rate after the self-cleaning process under UV light irradiation.

Materials and methods

Materials

The ceramic membrane material which was prepared by using kaolin powder (($Al_2Si_2(OH_5)_4$, < 1 μm) was purchased from Bg Oil Chem Sdn. Bhd., Malaysia. The polyethersulfone binder (PES, Radel A300, Ameco Performance, USA) was dried to ensure that no moisture was trapped, while N-methyl-2-pyrrolidone (NMP, Merck) was used as a solvent for the PES without further purification. The distilled water was

used as a coagulation bath during phase inversion process, and TiO_2 nanoparticles with a particle size of < 21 nm (Degussa P25, Evonik) were used as coating material on the ceramic membranes surface. The binder for the TiO_2 suspension was polyethylene glycol (PEG, molecular weight of 400) which was purchased from R&M Chemical. The humic acid (HA, Sigma Aldrich) was used as the solution model without further purification in determination of membrane solute rejection flux and rate. All the chemicals used in this study were in compliance with standard analytical grade.

Preparation of porous ceramic membranes coated with TiO_2

The ceramic membranes were prepared based on a specific composition using a phase inversion technique. The ceramic suspension was prepared by dissolving PES (15.0 g) in NMP (85.0 g) on a hot plate stirrer (500–550 rpm) for 4 h (60 °C), while distilled water (6.0 ml) was added into the polymer solution until a clear solution was obtained. Next, kaolin powder (60.0 g, 25 μm) was added into the polymer solution, and the stirring process was continued (48 h) until all the materials were completely dissolved and became a homogeneous ceramic suspension solution. The solution was subsequently poured into a bottle and left at room temperature (24 h) to release bubbles. Then, the solution was poured and cast on a glass plate (support) with a knife and placed into a coagulation bath (filled with 3 L of distilled water) at room temperature to allow the phase inversion to take place (5–10 min). The flat sheet membrane was then removed and dried at room temperature (24 h). The preparations of the ceramic membranes and coating with TiO_2 are illustrated (Fig. 1).

The ceramic membrane was subsequently dried in oven (4 h, 60 °C) to prevent the membrane from cracking due to temperature shock from rapid drying and heating during the sintering process. It was then sintered at high temperature by using furnace (PLF 140/5) to improve the strength of membranes. The temperature was increased (200 °C) at heating rate of 1 °C min^{-1} for 3 h to remove the water content. Next, the temperature was increased to 500 °C at heating rate of 1 °C min^{-1} for 6 h to remove organic binder. Increasing the temperature up to 1200 °C at heating rate of 1 °C min^{-1} for 2 h was final stage for mass suspension of kaolin powder. Finally, the temperature
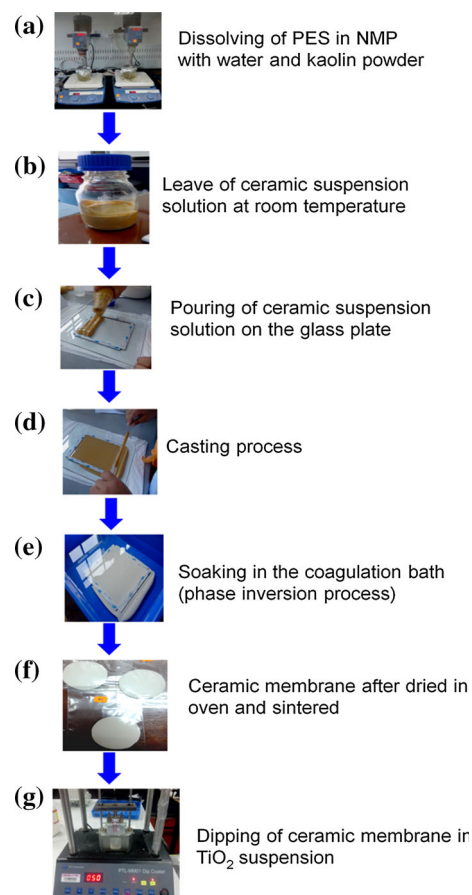

Figure 1 Preparation of ceramic membranes coated with TiO_2, procedures (**f**) and (**g**) was reversed in order to compare preparation techniques.

was cool down to room temperature for 24 h at cooling rate of 1 °C min^{-1} as illustrated (Fig. 2e).

A green body, without coating, acted as the control sample (GB-0). Next, TiO_2 nanoparticle suspensions with different concentrations (0.01, 0.03 and 0.05 wt%) were prepared. The TiO_2 nanoparticles were dispersed using a probe in distilled water and PEG (Sonic Dismembrator FB-50) to increase the stability of the TiO_2 nanoparticle dispersion process. The ceramic membrane was coated with the TiO_2 suspensions by using a dip-coating method (PTL-MM01 Dip Coater) with a speed of 50 mm/min (15 min). Later, the coated membrane was dried in an oven and sintered. So that the preparation methods could be compared, the technique was reversed, that is, the ceramic membrane was sintered first and then followed by dip coating with TiO_2. The composition of the ceramic suspension solutions and the coating of the ceramic membranes with TiO_2 are summarized (Table 1).
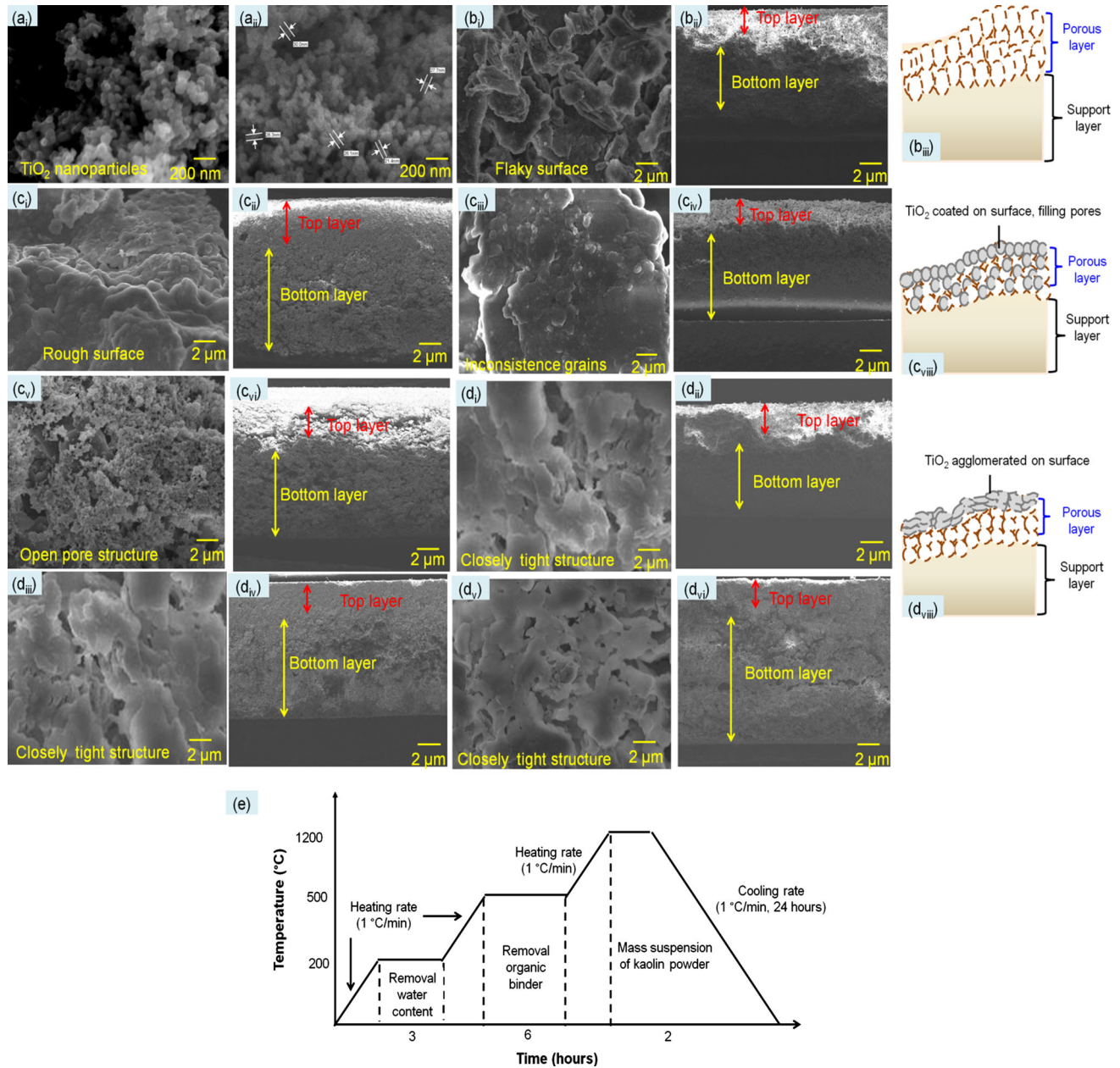
Figure 2 FESEM microstructure of (a_i) TiO$_2$ nanoparticles, (a_{ii}) TiO$_2$ nanoparticles size, (b_i) GB-0 surface, (b_{ii}) GB-0 cross section (b_{iii}) GB-0 cross section illustration, (c_i) GB-1 surface, (c_{ii}) GB-1 cross section, (c_{iii}) GB-3 surface, (c_{iv}) GB-3 cross section, (c_v) GB-5 surface (c_{vi}) GB-5 cross section (c_{viii}) all GBs cross section illustration, (d_i) SB-1 surface, (d_{ii}) SB-1 cross section, (d_{iii}) SB-3 surface, (d_{iv}) SB-3 cross section, (d_v) SB-5 surface (d_{vi}) SB-5 cross section (d_{viii}) all SBs cross section illustration and (e) sintering profile of ceramic membranes.

Characteristics of porous ceramic membranes coated with TiO$_2$

The cross-sectional morphology of the ceramic membranes was observed using field emission scanning electron microscopy (FESEM, JEOL JSM-7600F). A cross section of ceramic membrane was prepared by immersing the fractured membrane in liquid nitrogen. It was coated with platinum coating prior to characterization. The surface roughness of the membrane was also observed via atomic force microscopy (AFM, XE-Series Park Systems Model). The ceramic membrane was cut into a square shape (1.0 cm^2) before characterization.

Table 1 Composition of ceramic membrane materials coated with TiO_2

Sample code	Kaolin (g)	NMP (g)	PES (g)	Water (ml)	TiO_2 (wt%)	Dip coating of TiO_2	Duration of coating (minutes)
GB-0	60.0	85.0	15.0	6.0	–	–	–
GB-1	60.0	85.0	15.0	6.0	0.01	Before sintering	15
GB-3	60.0	85.0	15.0	6.0	0.03	Before sintering	15
GB-5	60.0	85.0	15.0	6.0	0.05	Before sintering	15
SB-1	60.0	85.0	15.0	6.0	0.01	After sintering	15
SB-3	60.0	85.0	15.0	6.0	0.03	After sintering	15
SB-5	60.0	85.0	15.0	6.0	0.05	After sintering	15

The shrinkage percentage that occurred during the sintering process was measured by recording the diameter and thickness of the ceramic membrane before and after the sintering process. The percentage of shrinkage is calculated (Eq. 1):

$$\frac{D_i - D_f}{D_i} \times 100 \tag{1}$$

where D_i is the initial diameter/thickness before sintering and D_f is the diameter/thickness after the sintering process. The diameter/thickness was measured using a vernier caliper (digimatic, Mitutoyo), and average values were taken to attain the final value for each membrane.

The porosity of the ceramic membrane was measured using a porosity weight scale (Mettler Tuledo). Archimedes' principle was used for the calculation of the porosity and bulk density of the ceramic membranes. Firstly, the ceramic membrane was weighed in a dry state. It was then submerged in liquid, removed from the liquid and weighed. Finally, the obtained values are substituted to calculate the porosity (Eq. 2) and density (Eq. 3):

$$\frac{W_w - W_d}{W_w - W_s} \times 100 \tag{2}$$

$$\frac{W_d}{W_d - W_s} \times 100 \tag{3}$$

where W_d is the weight of the dry ceramic membrane and W_s is the weight of the ceramic membrane after submersion and W_w is the weight of the ceramic membrane after removal from the liquid. A porosity test is also used to determine the percentage of water absorption (Eq. 4):

$$\frac{W_d - W_s}{W_d} \times 100 \tag{4}$$

The mean pore radius (r_m, in μm) of the ceramic membrane was determined using the filtration velocity method. According to the Guerout–Elford–Ferry equation, r_m is determined experimentally (Eq. 5):

$$\sqrt{\frac{(2.9 - 1.75\varepsilon) \times 8\eta\ell Q}{\varepsilon \times A \times \Delta P}} \tag{5}$$

where η is water viscosity (8.9×10^{-4} Pa s), ℓ is membrane thickness (m), Q is volume of permeate water per unit time ($m^3 s^{-1}$), A is the effective membrane surface area (m^2) and ΔP is operational pressure (ρgh).

Performance characterization of porous ceramic membranes coated with TiO_2

The PWF of ceramic membranes and rejection were measured by the gravity pressure method with dead-end filtration using our design system [9–11]. The ceramic membrane was cut to a 45.0 mm diameter size for both characterizations. Distilled water was used during testing, and the PWF is calculated (Eq. 6):

$$\frac{Q}{(A \times \Delta t)} \times 100 \tag{6}$$

where Q is the volume of water permeated (L), PWF is permeation water flux (L $m^{-2} h^{-1}$), A is the effective membrane surface area (m^2) and Δt is permeation time (hours). The rejection rate characterization was obtained by using the HA solution at a specific pressure (2 bar) and concentration (0.2 gL^{-1}). The concentration of HA permeation (C_P) and concentration of HA feed (C_F) during filtration were measured using the UV–Vis spectrophotometer (Perkin-Elmer Lamda 25). Then, the rejection rate is determined (Eq. 7):

$$\left[1 - \left(\frac{C_p}{C_F}\right)\right] \times 100 \tag{7}$$

Next, the fouling was achieved by running HA as feed through the ceramic membrane surface. The fouling test was performed (2 h), and the readings were taken (every 10 min). Later, the self-cleaning evaluation was performed after fouling occurred on the ceramic membrane surface. The ceramic membrane was placed under 160 watt of UV radiation (15 min) to allow the photocatalytic reaction and self-cleaning of the ceramic membrane to occur. After that, the rejection characterization was repeated (10 min) using HA. Finally, the change in the membrane surface was observed.

Results and discussion

Morphology of porous ceramic membranes coated with TiO_2

Cross-sectional morphology analysis of the coated TiO_2 nanoparticles is very important to ensure their ability to adhere to the membrane surface. Changes in the asymmetric porous ceramic membrane structure from top to bottom layers for both membranes with TiO_2 coating were observed for the two techniques of coating; coating before and after the sintering process. Basically, the TiO_2 nanoparticles showed uniform shape and particle size (21.4–30 nm) (Fig. 2a_i–a_ii). After the sintering process, the uncoated ceramic membrane (GB-0) had a slightly flaky, homogenous surface. The cross section of GB-0 revealed an asymmetric structure with dense top, porous layer and a slightly porous layer toward the bottom support layer. This indicates that the membrane structure that had undergone the sintering process has attached particles, which resulted in the diminishing of pores and the stacking of loose particles (Fig. 2b_i–b_iii).

The surface and cross section of the green body ceramic membrane coated with different concentrations of TiO_2 nanoparticles before sintering at 0.01 wt% (GB-1), 0.03 wt% (GB-3) and 0.05 wt% (GB-5), exhibited highly porous surface coating with uniform condition (Fig. 2c_i–c_vi). In fact, the dense penetrated layer was shown to be longer than that of membranes coated with TiO_2 after the sintering process (SB). This may be related to the fact that TiO_2 particles can possibly penetrate deeper into all GB membranes during the sintering process. This would be due to the recombination of loose particles, that

eventually create more space, or void, that can be filled in by TiO_2 nanoparticles inside the main substrate body [12, 13].

The GB-1 surface shown slightly higher porosity which created a rougher surface attributing to a lower concentration of TiO_2 nanoparticles coated onto the surface. Meanwhile, GB-3 showed good morphology with uniform surface due to the optimum concentration of TiO_2 nanoparticles that have penetrated deeper into all GB membranes. Membranes coated with higher concentrations of TiO_2 nanoparticles exhibited a dense porous structure at their outer surface since more particles are able to penetrate the membrane interior. Simultaneously, some of the nanoparticles remain at the coating layer, which slightly reduces the pore size. This phenomenon can be observed on samples with a denser coat of TiO_2 nanoparticles such as GB-5, which exhibited very compact structure compared to GB-1 and GB-3, indicating that higher particle concentration in the coated layer strongly influences the surface morphology structure. Therefore, the cross section of all GB membranes showed that porosity at the outer surface is maintained indicating the ability of TiO_2 to penetrate inside the pores main substrate (Fig. 2c_viii).

The surface and cross section of porous ceramic membranes, coated with TiO_2 nanoparticles onto a sintered body, were labeled based on different concentrations of TiO_2 nanoparticles which are 0.01 wt% (SB-1), 0.03 wt% (SB-3) and 0.05 wt% (SB-5), respectively. These membranes were observed to be totally agglomerated with large stacking particles (Fig. 2d_i–d_vi). This may be attributed to the slow penetration of TiO_2-coated particles into the denser sintered body (SB) membrane. It is, in fact, nearly impossible for TiO_2 nanoparticles to penetrate the sintered body and has the tendency to cause agglomeration on the outer surface and in due course creating nonhomogeneous structure. The observed morphology was found to be similar to that obtained by a previous study on tubular ultrafiltration ceramic membranes based on immobilized TiO_2 nanoparticles on macroporous clay-alumina support [14]. Observation of membrane morphology, starting with low concentrations of TiO_2 in the coating medium (SB-1), showed lower agglomeration effect in contrast to that of high concentrations of TiO_2 coated onto SB-2 and SB-3 membranes. As the concentration of TiO_2 nanoparticles in the coating suspension is increased, the morphology

becomes densely packed with agglomerated particles which are linked to the mechanism of sintering. When the membrane was sintered at higher concentration of TiO$_2$ nanoparticles suspension, the membrane tends to combine loose particles and form solid structure as well as for the elimination of pore networking. This dense agglomeration of particles inside membrane decreases the penetration of TiO$_2$ nanoparticles layer inside the body (Fig. 2d$_{viii}$).

As shown by the sintering curve, the thermal heat treatment process was implemented to remove water content and organic matter at a lower temperature, beside improved the cross-sectional morphology of membranes (Fig. 2e). When the GB membranes were coated before sintering, the water was only removed at the drying stage, but the structure was still in loosely packed or open-structure form and thus able to penetrate deeply inside by TiO$_2$ nanoparticles during sintering at a later stage. This will create more pores elimination and generated a close, tightly-grained structure at high temperature. However, when the membrane was coated after sintered, a dense agglomeration of particles with a low penetration layer inside the body was generated. This demonstrates that the interface structure of this membrane is weak due to slow and difficult penetration of the coating medium. In the coating preparation stage, the generation of interface structure with strong adhesive bonding and attachment is very important to ensure that the coating layer cannot easily peel off from the main substrate body. Although the GB ceramic membrane is considered a weak body with a high erosion or deterioration potential during coating (as it is still on loose particles), it can be sustained when the coating occurs onto a green body. This could be due to better absorption capacity by structure with higher porosity. This mechanism can be improved by extending the drying stage to remove all water and unwanted materials in order to create a more porous structure.

Surface roughness of porous ceramic membranes coated with TiO$_2$

Surface texture analysis is also important in understanding the properties of ceramic membranes that have gone through the coating process using different routes. Determination of surface roughness by AFM measuring is important as it relates to the ability of the membrane to prevent the fouling mechanism and its antifouling properties for separation applications. The three-dimensional topographical images are measured, and the mean surface roughness (R_a) values are recorded (Fig. 3, Table 2). The brightest regions represent the highest points of the ceramic membranes surface, while the darkest regions correspond to the pore entrances. The controlled sample (GB-0) had the highest surface roughness value due to the existence of empty pores on the membrane surface after it was sintered.

As can be observed in the plotted image (Fig. 3h), the value of surface roughness for the samples coated with TiO$_2$ after sintering (SB-1, SB-3 and SB-5) is higher compared to the green body samples coated before sintering (GB-1, GB-3 and GB-5). This could be due to the agglomeration of TiO$_2$ nanoparticles in the SB structure that has a strong tendency to form a rougher surface compared to the GB structure. The GB structure is dominated by the pore structure due to the penetration of TiO$_2$ nanoparticles further inside the body. Both of the membrane showed similar trend of reduced surface roughness due to increased coated layer concentration. The increased TiO$_2$ nanoparticles concentration effectively closes the pores at the outer surface of the uncoated membrane reducing its surface roughness.

As can also be observed, the surface roughness of GB (GB-1, GB-3 and GB-5) showed that the different degrees of surface roughness among these three membranes are lower compared to membranes coated after sintering. Reduction of surface roughness through the penetration of TiO$_2$ particles was not significant attributed by a loose structure with open pores inside membrane that enable higher pore-infiltration. Furthermore, the agglomeration of TiO$_2$ nanoparticles attaching to the surface of SB-1, SB-3 and SB-5 membranes coated after sintering, makes the surface slightly rougher compared to GB membranes. Basically, lower surface roughness will provide a smaller effective area of permeation compared to membranes with higher surface roughness [15]. However, although higher surface roughness can potentially increase permeation performance of the ceramic membrane, it can concurrently contribute to the fouling of the surface area due to the curvature and intricate shapes that tend to trap pollutants or foulants [15].
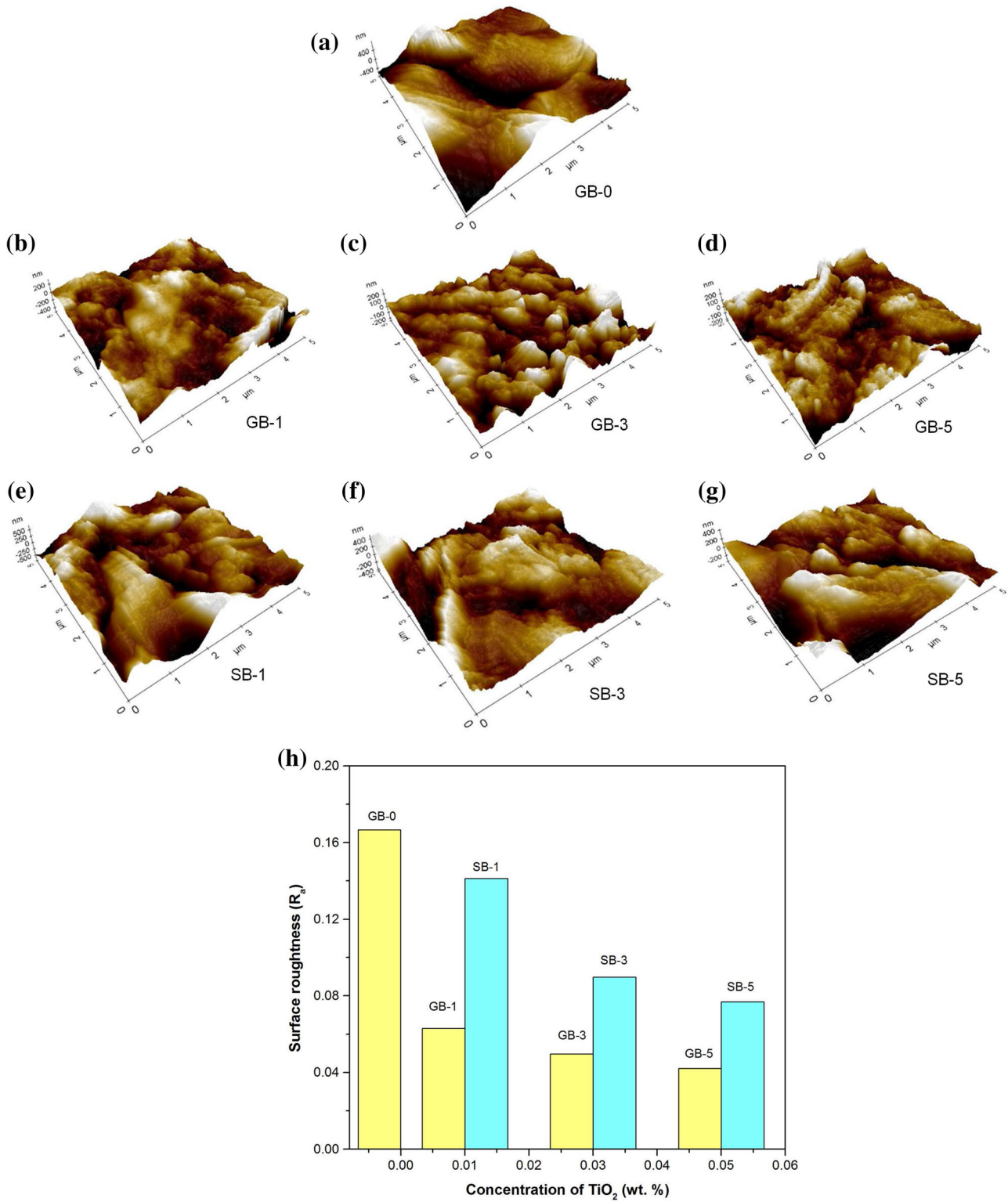
Figure 3 Surface topography of (**a**) GB-0, (**b**) GB-1, (**c**) GB-3, (**d**) GB-5, (**e**) SB-1, (**f**) SB-3, (**g**) SB-5 and (**h**) surface roughness of ceramic membranes.

Table 2 Summary of ceramic membranes with different TiO$_2$ coating routes: characterization, properties and performance

Sample code	Surface roughness, R$_a$ (μm)	Diameter shrinkage (%)	Thickness shrinkage (%)	Weight loss (%)	Porosity (%)	Density (g cm^{-3})	Water absorption (%)	Mean pore radius (μm)	Permeation of PWF (Lm^{-2}h^{-1})	Rejection rate (%)	Self-cleaning performance			
											Rejection flux (Lm^{-2}h^{-1})		Rejection rate (%)	
											Before UV lamp	After UV lamp	Before UV lamp	After UV lamp
GB-0	0.17	9.84	9.93	32.08	71.50	2.06	49.12	0.01890	98.09	83.68	49.05	49.05	97.83	97.83
GB-1	0.07	8.87	9.77	31.70	69.12	2.20	45.17	0.01486	109.41	85.92	64.14	75.46	98.27	98.34
GB-3	0.05	8.68	9.53	31.46	68.09	2.21	44.67	0.01457	128.28	86.06	75.46	94.32	98.34	98.56
GB-5	0.04	8.51	9.38	31.05	66.64	2.28	43.77	0.01451	116.96	86.14	67.91	86.78	98.41	98.63
SB-1	0.14	9.84	9.86	32.05	71.20	2.07	47.69	0.01803	98.09	84.12	52.82	56.59	97.98	98.05
SB-3	0.09	9.79	9.85	31.79	71.06	2.11	46.59	0.01676	101.87	85.70	56.59	60.37	98.12	98.19
SB-5	0.08	9.70	9.78	31.78	69.73	2.19	45.24	0.01657	101.87	85.85	56.59	64.14	98.19	98.27

Physical properties of porous ceramic membranes coated with TiO$_2$

During sintering process, it is crucial to prevent excessive shrinkage. Therefore, shrinkage needs to be measured to prevent failure or leaking of the ceramic material. The range of allowable tolerance for ceramic shrinkage is within 3–5%. Both the diameter and thickness were measured to determine the percentage of shrinkage. The results showed significant shrinkage of the ceramic membranes, particularly after the sintering process. This is a notified drawback in ceramic membranes, but it can be solved by modification of production method, i.e., mineral coating, which endows the membrane with outstanding curling resistance, mechanical stability and which meets the requirements of filtration for water treatment [16].

In this study, excessive shrinkage has obviously occurred in the membrane sample coated with TiO$_2$ after sintering (SB-1, SB-3 and SB-5) due to slow or weak penetration of the coating medium into the compact sintered body. As aforementioned, this accumulation of TiO$_2$ at the outer surface layer could lead to the excessive shrinkage in all SB membranes. The higher shrinkage percentage of these membranes could be due to the coating medium being concentrated in the liquid phase at which it can evaporate easily throughout the drying and sintering process. In contrast, membranes coated before sintering (GB-1, GB-2 and GB-3) show slightly reduced shrinkage. This is because the penetration of the coating medium onto the loose green body allows the filling mechanism, enabling the green body structure to compact and resulting in lower shrinkage during sintering. Thus, for all GB membranes, shrinkage was slightly lower than for SB membranes.

The tendency for shrinkage was decreased as the concentration of the coating medium was increased. This can be observed in the plotted results for both diameter and thickness. The result can be vividly seen in the thickness of the GB membranes (Fig. 4A(a–b)) revealing the ability of a green body to absorb the coating medium at a higher concentration of TiO$_2$ particles that lead to a greater particle-filling effect which subsequently retards the drastic shrinkage. The degree of diameter and thickness shrinkage is proportional to weight loss, where the weight losses of all SB membranes were higher compared to all GB membranes. This revealed that compact sintered bodies, which create accumulation of coating due to
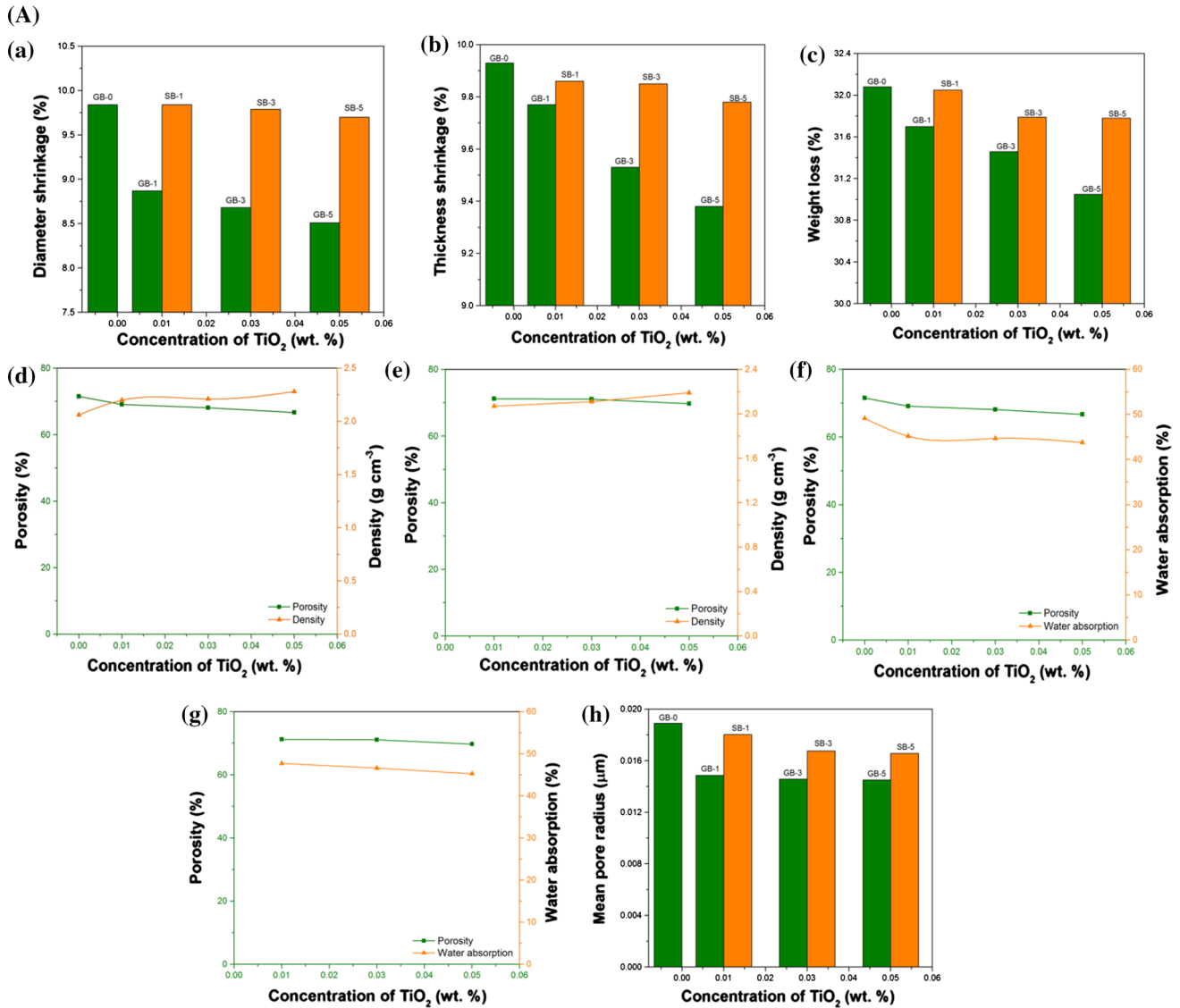
Figure 4 (**A**) Physical properties of ceramic membranes (**a**) shrinkage of diameter, (**b**) shrinkage of thickness, (**c**) weight loss, (**d**) porosity-density of GBs, (**e**) porosity-density of SBs, (**f**) porosity-water absorption of GBs, (**g**) porosity-density of SBs and (**h**) mean pore radius and (**B**) shrinkage phenomena in ceramic membranes (**a**) GB-0, (**b**) GB coated with TiO_2 before sintering and (**c**) SB coated with TiO_2 after the sintering process.

low penetration of the coating medium, does not only show higher shrinkage, but also greater weight loss (Fig. 4A(c)). Furthermore, the weight loss is decreased as the concentrations of TiO_2 increase for the different TiO_2 coating and sintering methods.

The porosity of SB membranes is higher compared to GB membranes, whereas the density plot for both GB and SB membranes shows a similarity. As the concentration of the coated layer is increased, the porosity is reduced due to the incremental filling effect of the TiO_2 nanoparticles for both types of membranes. As the porosity increases, the density

will be consequently reduced. This trend is concurring with other density and porosity plots of porous materials that similarly showed inverse pattern between these two parameters (Fig. 4A(d–e)). Other measured parameters, such as water absorption, also strongly correlated with the porosity value. Thus, as the increasing concentrations of TiO_2 evidently reduced porosity, a lower surface area for water absorption is created (Fig. 4A(f–g)). Moreover, these particular trends in porosity, density and water absorption are similar to those observed in a previous study by Hristov et al. [17].
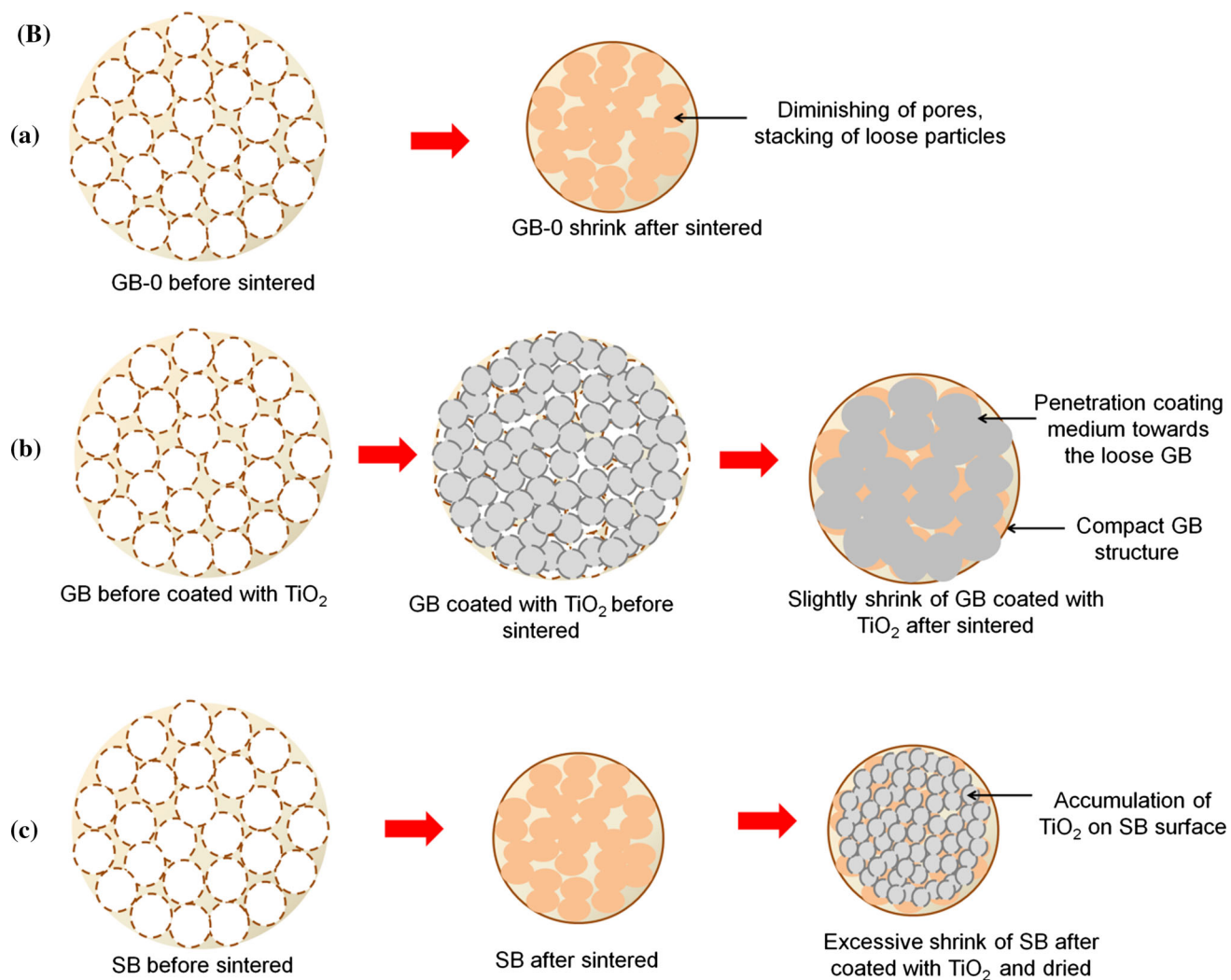
(B)

(a)

GB-0 before sintered

Diminishing of pores, stacking of loose particles

GB-0 shrink after sintered

(b)

GB before coated with TiO₂

GB coated with TiO₂ before sintered

Penetration coating medium towards the loose GB

Compact GB structure

Slightly shrink of GB coated with TiO₂ after sintered

(c)

SB before sintered

SB after sintered

Accumulation of TiO₂ on SB surface

Excessive shrink of SB after coated with TiO₂ and dried

Figure 4 continued.

Another imperative physical property that should not be overlooked is the mean pore radius. The mean pore radius was found to decrease as the concentration of TiO_2 increased for both GB and SB membranes (Fig. 4h). The good TiO_2 particle arrangement coated on GB-1, GB-3 and GB-5 membrane structures had generated smaller pores due to the filling of TiO_2 in the pores. This dense packing arrangement had indirectly decreased the porosity as well as the mean pore radius. Thus, as the TiO_2 particles increased in a suspension, more of the particles will be trapped inside the pores of the ceramic membrane. As a result, this will decrease the porosity, the mean pore radius and the percentage of water absorption of GB-1, GB-3 and GB-5 membranes. Although the mean pore radiuses of SB membranes were higher compared to GB membranes, relative to their porosity values, the TiO_2 nanoparticles were accumulated on the surface. These values also decreased as TiO_2 concentrations increased. Accumulation of higher TiO_2 concentrations on the compact sintered body surface consequently decreased the surface area for TiO_2 penetration as well as the mean pore radius.

In this study, the control sample showed higher values for shrinkage, weight loss, porosity, mean pore radius and water absorption, but lower density (GB-0 membrane) compared to GB-1, GB-3 and GB-5 membranes after sintering. These differences are due to the presence of pores, the diminishing of pores and the stacking of loose particles inside the naked membrane (without coating), after the sintering process. The performance of the membrane was
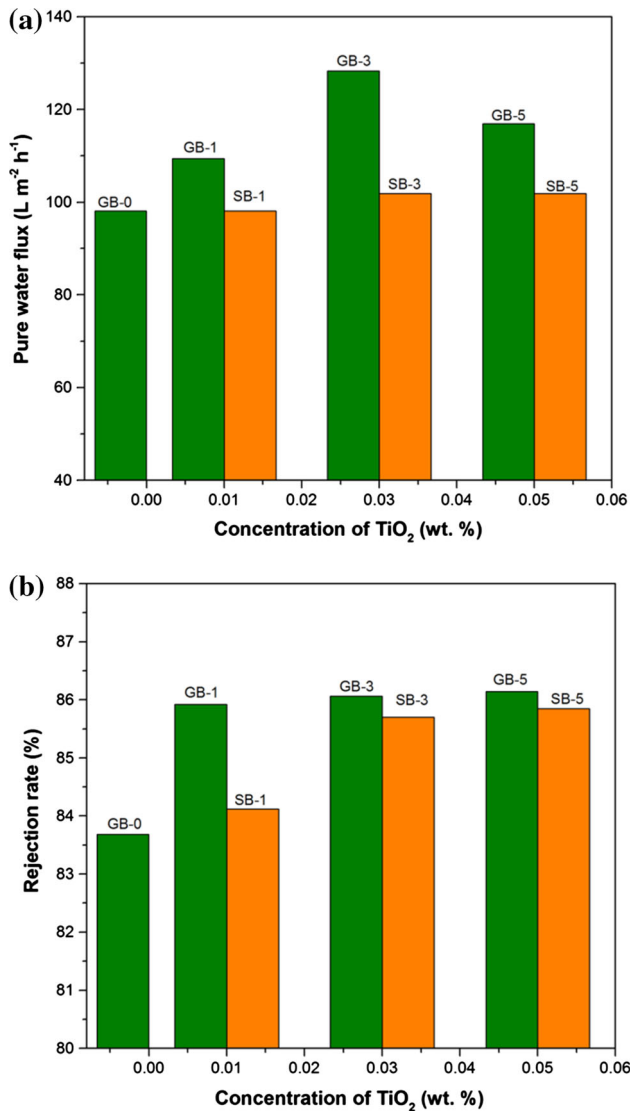
Figure 5 Ceramic membranes (**a**) permeation of water flux and (**b**) rejection rate.

enhanced when the physical properties of the membrane before and after coating with TiO_2 are compared. Generally, increasing the concentrations of TiO_2 does not significantly influence all the physical properties of both sintering methods, but there is still a change in values (Table 2). All the physical characterizations were found to be correlated with each other and strongly depend on the morphology and surface roughness of the ceramic membranes.

Permeation of pure water flux and rejection rate of porous ceramic membranes coated with TiO_2

Permeation of pure water flux (PWF) and rejection rate are related to the ability of a ceramic membrane to function as a separator (filter). The ceramic membrane has selective permeability, which means that the membrane will allow certain substances to pass through, while forming a barrier (rejection) against others. Normally, the relationship between PWF and the rejection rate strongly depends on the morphology, surface roughness and physical properties of the membranes. In this study, the PWF and rejection rate of ceramic membranes coated with TiO_2 before sintering (GB-1, GB-3 and GB-5), or coated onto a ceramic membrane in a green state, are higher in comparison with membranes coated with TiO_2 after being sintered (SB-1, SB-3 and SB-5) (Fig. 5a, Table 2). Although the porosity influenced the permeation PWF, the effect of TiO_2 coating cannot be ignored. Previous studies have shown the interconnectivity of pores inside membranes was increased due to larger porous membrane surface, enhanced PWF and reduced indirect solute rejection [18].

However, the permeation rates of GB-1, GB-3 and GB-5 ceramic membranes were found to be reversed with slightly lower porosity and surface roughness which enabled them to generate a slightly higher permeation rate. This could be attributed to the formation of a uniform layer of TiO_2 nanoparticles in the coating that is able to penetrate inside the membrane structure resulting in a reduction in accumulated particles. This occurred when the coating step was conducted on a green body. In this case, the coated medium easily penetrated the body. This was followed at a later stage by a rearrangement of particles during sintering. This homogenous structure of the coated layer provides low resistance to the permeation path.

The lower porosity values for GB membranes have proven their ability to generate a higher HA rejection rate as compared to SB membranes. This can be clearly seen in the rejection plot, which shows a higher concentration of the coated layer (Fig. 5b, Table 2). Thus, as the concentration of the coated medium is increased, the rejection value tends to also increase indicating that only small amounts of pollutants can pass through the membrane. Low rejection can be attributed to a number of factors such as
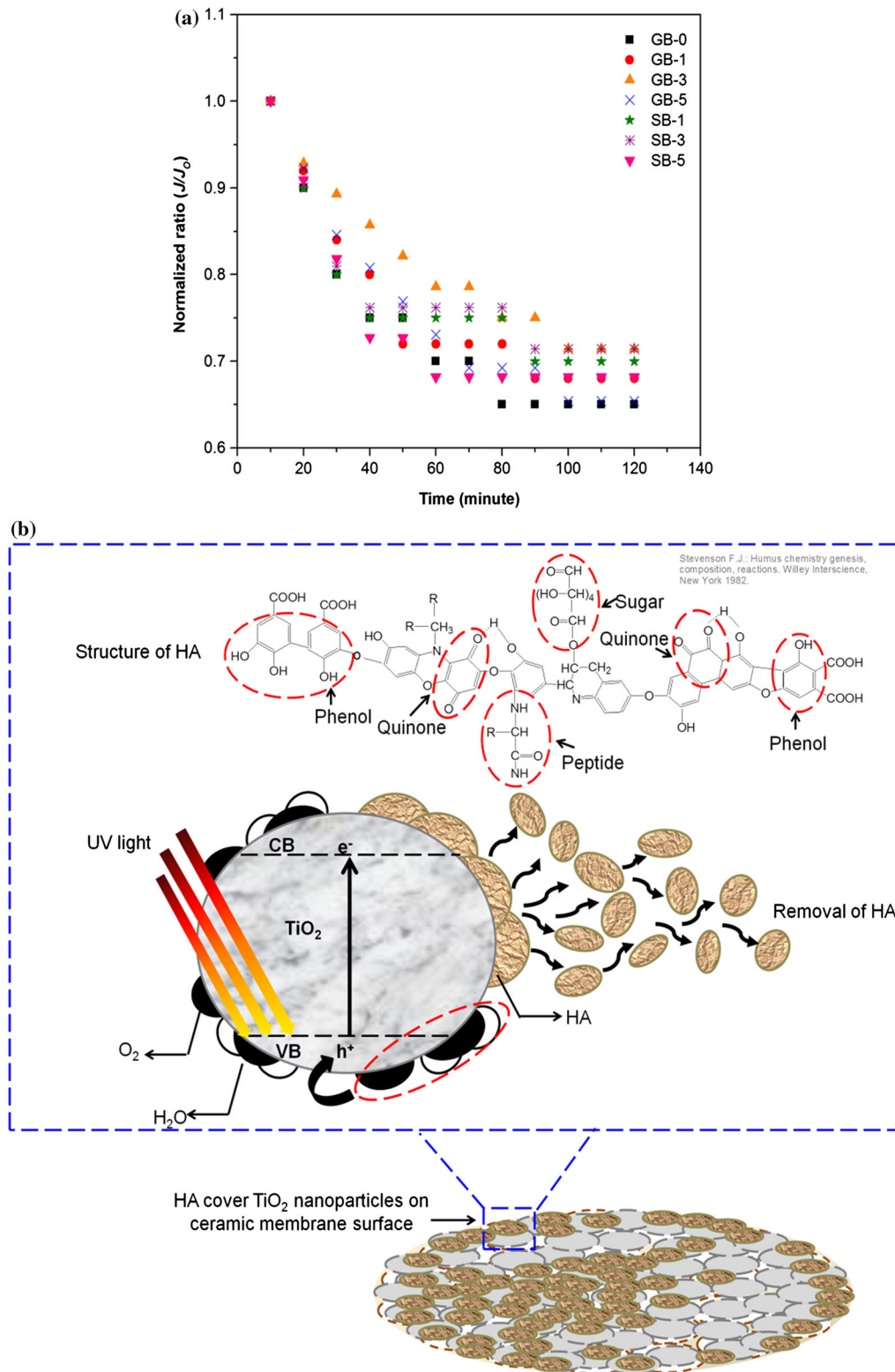
Figure 6 (a) Normalized flux ratio of GB-0, GB-1, GB-3, GB-5, SB-1, SB-3, SB-5 ceramic membranes and (b) the proposed photocatalytic mechanism of TiO$_2$ and removal of humic acid from porous ceramic membranes. The structure of humic acid was redrawn using ChemDraw Ultra, based on Ref. [21].

the adsorption of ability of membranes, the trapping of organic species on the membrane surface or other related factors [19]. This contradicting relationship between permeation and porosity, as well as surface roughness, is mostly influenced by the condition of the coating layer. Furthermore, TiO_2 nanoparticles on SB-1, SB-3 and SB-5 ceramic membrane surfaces decrease both the PWF and the rejection rate. Even the porosity of SB membranes is higher in comparison with GB membranes. The accumulation of TiO_2 nanoparticles can result in high resistance to both permeate flow and rejection rate.

The average rejection rate of HA obtained from GB-0 membranes is attributed to the presence of a porous structure on the membrane interior, which continuously attracts water permeates without blockage. The high porosity of GB-0 membranes, as well as their increased HA rejection rate, is due to the interconnectivity of pores inside the membrane, which was observed in the cross-sectional morphological analysis, as discussed earlier (section "Morphology of porous ceramic membranes coated with TiO_2"). The sufficiently small size of membrane pores had prevented HA from entering the pore length due to the blocking action of solute particles [20].

Antifouling and self-cleaning of porous, ceramic TiO_2-coated membranes

Fouling is a type of resistance that is caused by the formation of a cake- or gel-like layer on the membrane surface and/or inside the pores. It adversely affects the ability of membranes to filter impurities. In this study, HA was used as model foulant compound in replacement to natural organic matter (NOM) that was normally present in real wastewater. Phenols and phenolic compounds are some of the major organic contaminants in industrial wastewater [3]. The normalized flux ratio is reduced with time (Fig. 6a). As can be seen, the ability to filter HA during separation depends on the TiO_2 concentration and the effect of the different coating routes of the ceramic membrane. By and large, normalized flux results showed that the membrane coated before sintering, GB, had slightly higher resistance toward fouling. The plotted results showed a slightly lower drop in this value compared to the SB membrane that was coated after sintering. As discussed earlier, the GB membrane offers better coating of TiO_2 nanoparticles. This results in homogenous structure with a lower agglomeration effect, which creates better distribution of TiO_2 particles.

Moreover, lower surface roughness and a homogenous coating layer increased the antifouling properties, as discussed earlier (section "Surface roughness of porous ceramic membranes coated with TiO_2"), by reducing the amount of pollutants trapped in this area. Increasing the coating concentration of TiO_2 particles had simultaneously increased the antifouling properties of both coated membranes, indicating that TiO_2 particles had strongly affected the antifouling effect on the HA medium. The results for membranes coated before and after sintering were observed within by GB-3, GB-5, GB-1, and, SB-5, SB-3 and SB-1, respectively. In contrast, the control sample (GB-0) had the lowest normalized flux ratio, due to the nonexistence of the self-cleaning effect offered by TiO_2 nanoparticles.

Fouling problem can be effectively solved by varying the coating technique such as providing coating layer that fortifies the antifouling properties of the membrane. This can be achieved through self-cleaning mechanism. Normally, HA consists of a skeleton of alkyl/aromatic units, which are cross-linked by different functional groups such as carboxylic, phenolic, and alcoholic hydroxyls, ketone and quinone groups. In aqueous solution mediums, the negative charge of HA is attributed to the carboxyl and phenolic groups, while the solubility depends on the number of –COOH and –OH groups [21, 22]. The self-cleaning and removal of HA are facilitated by a photocatalytic reaction of the TiO_2 coated on the membrane surface under illumination by UV light [22–24].

The electron (e^-) at the conduction band (CB) and the hole (h^+) at the valence band (VB) are generated when TiO_2 nanoparticles on the ceramic membrane surface/inside pores interact with UV light (Fig. 6b). The trapping of holes by water (H_2O) or oxygen (O_2) on TiO_2 nanoparticles surface produces H^+ and $HO^.$. Both of these useful radicals are oxidation agents that can obliterate HA on the membrane surface [7]. The HA molecule is attacked by $HO^.$ due to the addition of a hydroxyl or hydrogen extraction effect. Conversion of HA to CO_2 and H_2O can occur by different routes such as phenols-quinones-acids-CO_2 [21]. The hydroxycyclohexadienyl radicals ($HCHD^.$) are produced through the addition of $HO^.$ to aromatic sites of HA [25]. Further oxidation of $HCHD^.$ will generate ring-opened products. Additionally, the unsaturated
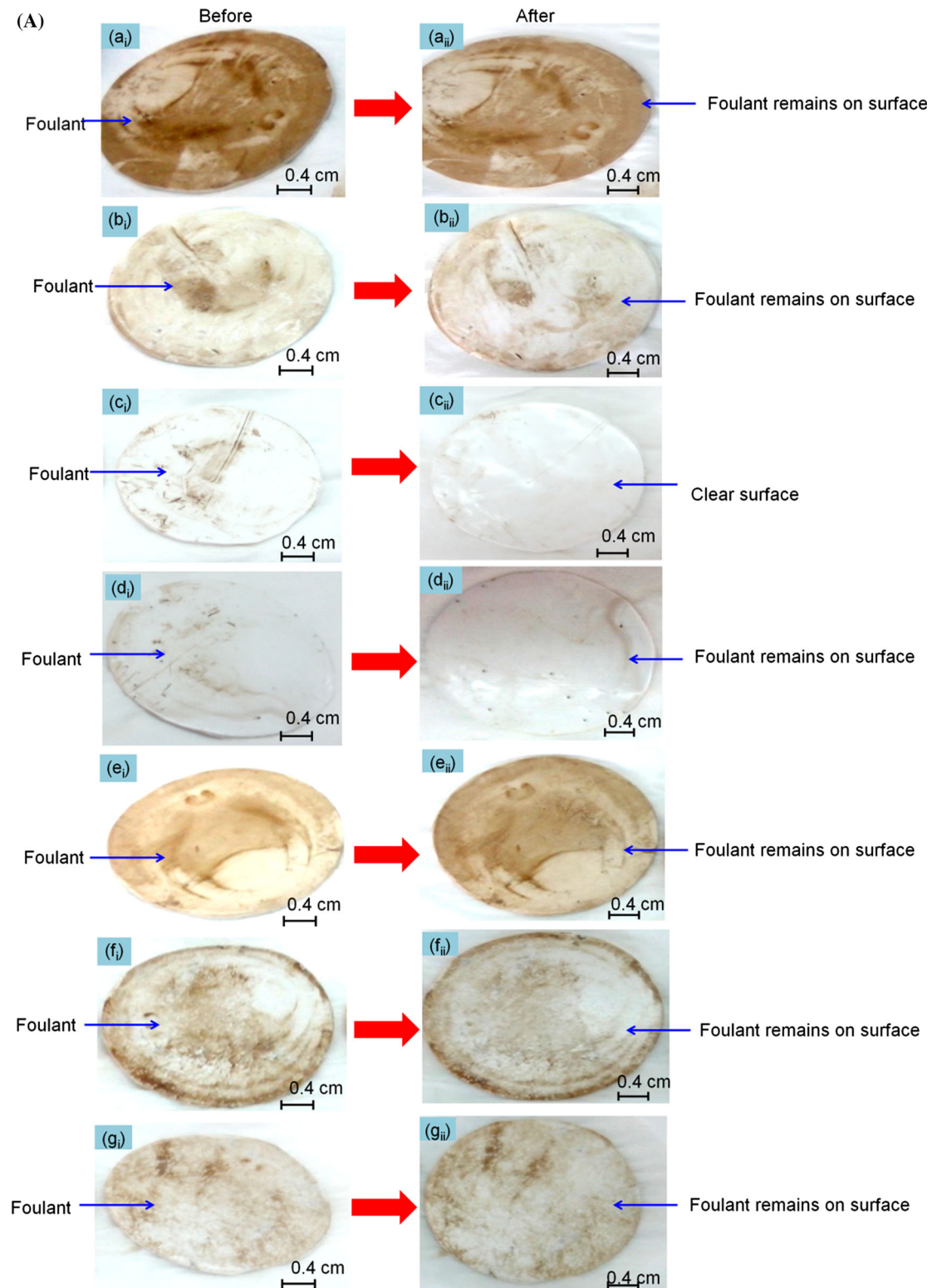
Figure 7 (**A**) Self-cleaning process of (**a_i**) GB-0 membrane before (**a_ii**) GB-0 surface after, (**b_i**) GB-1 membrane before (**b_ii**) GB-1 surface after, (**c_i**) GB-3 membrane before (**c_ii**) GB-3 surface after, (**d_i**) GB-5 membrane before (**d_ii**) GB-5 surface after, (**e_i**) SB-1 membrane before (**e_ii**) SB-1 surface after, (**f_i**) SB-3 membrane before (**f_ii**) SB-3 surface after, (**g_i**) SB-5 membrane before and (**g_ii**) SB-5 surface after, (**B**) example illustrations of ceramic membrane surface self-cleaning before, during, after exposure to UV light and removal of HA on (**a**) GB-0, (**b**) GB-3 and (**c**) SB-3, (**C**) performance of ceramic membranes before and after exposure to UV light (**a**) rejection flux and (**b**) rejection rate.
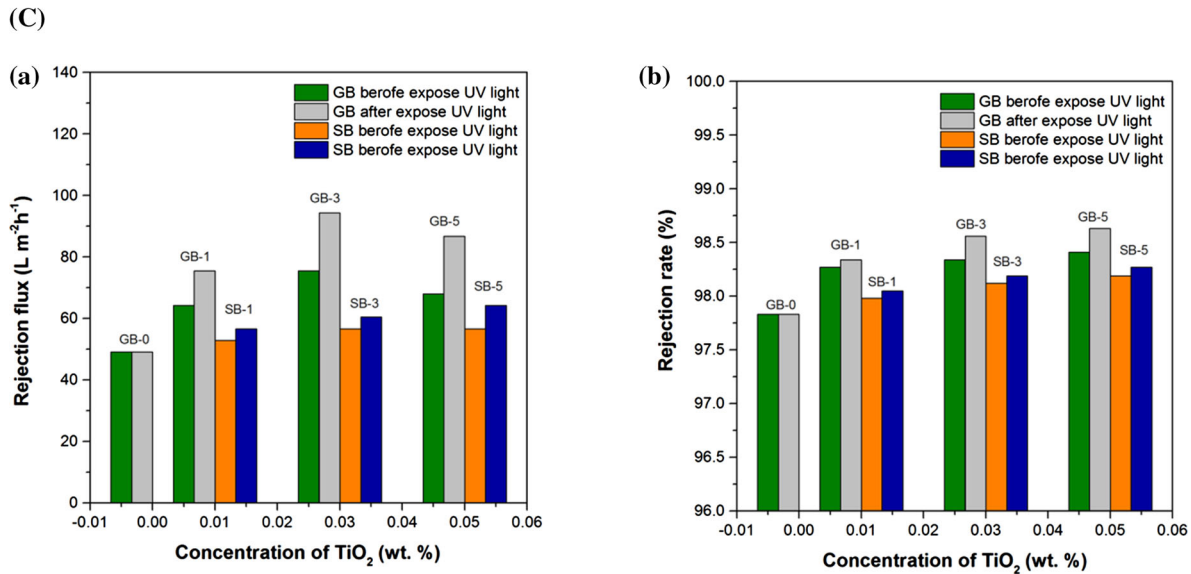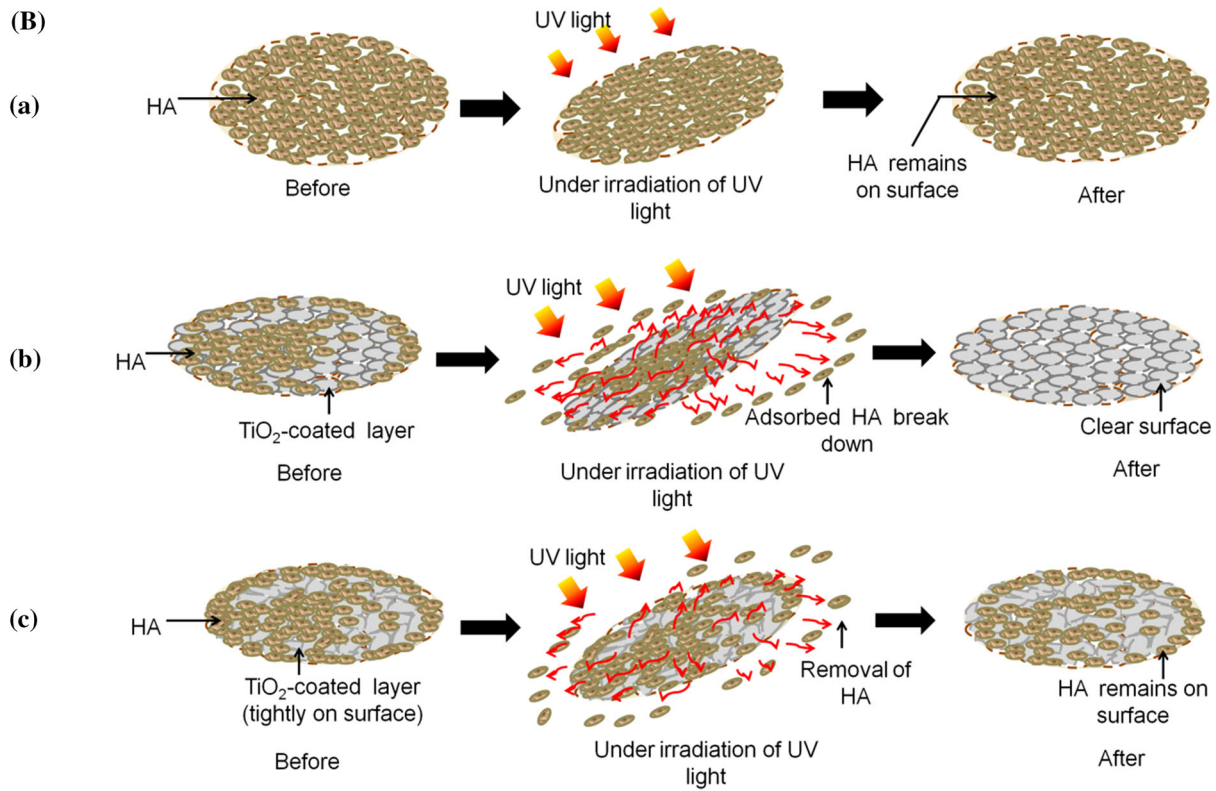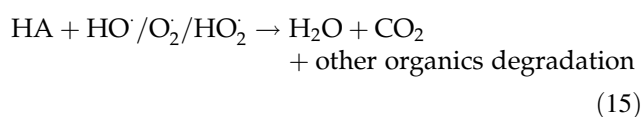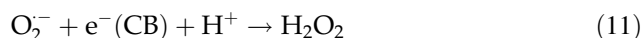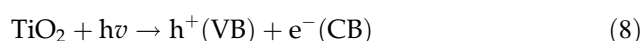
(B)

(C)

Figure 7 continued.

groups in HA (aromatic and vinyl groups) produced dialkyl peroxide and auto-degraded $RO^{.}$ and epoxide.

The formation of CO_2 and ring-opened products has the potential to decrease molecular size, while the reaction of $^{.}OH$ radicals was found to increase the

fraction of HA with less hydrophobic and aromatic natures [26]. The reactions between HA and radical species (O_2^-, $HO_2^.$ or $HO^.$) generated intermediate substances and finally formed CO_2 simultaneously with decomposition of the organic materials [22]. Essentially, the photocatalytic mechanism of TiO_2 is dependent on various parameters (crystallinity, surface area, particle size, defect sites and surface charge), as well as substrate–surface interactions [27]. In this study, this mechanism is proposed as follows (Eqs. 8–15) [22]:

$$TiO_2 + h\nu \rightarrow h^+(VB) + e^-(CB) \tag{8}$$

$$h^+(VB) + OH^- \rightarrow HO^. \tag{9}$$

$$e^-(CB) + O_2 \rightarrow O_2^- \tag{10}$$

$$O_2^- + e^-(CB) + H^+ \rightarrow H_2O_2 \tag{11}$$

$$H_2O_2 + e^-(CB) \rightarrow HO^. + OH^- \tag{12}$$

$$O_2^- + H^+ \rightarrow HO_2 \tag{13}$$

$$HO_2^. + H^+ + e^-(CB) \rightarrow HO^. + OH^- \tag{14}$$

$$HA + HO^./O_2^-/HO_2^. \rightarrow H_2O + CO_2$$
$$+ \text{ other organics degradation} \tag{15}$$

In this work, analysis was conducted by exposing both coated membranes in the HA medium to UV light illumination. Observation was carried out based on changes to the surface of membranes before and after exposure to UV illumination. As expected, the non-existence of the TiO_2 coating for the GB-0 membrane, which means that it will not generate a photocatalytic mechanism. This will result in the accumulation of HA on the membrane surface as well as a reduction in flux (Fig. 7A(a), B(a)). Thus, both of the flux and rejection rates remained unchanged regardless of exposure to UV light occurred before or after (Figure 7C, Table 2). Further investigations, based on HA rejection flux and rate, were also conducted before and after exposure to UV light illumination.

The HA rejection flux and rate for all GB membranes are higher compared to all SB membranes. This could be due to the lower surface roughness and uniform coating structure, which may facilitate the elimination of foulants during the photocatalytic activity. All of the coated membranes were evaluated at different concentrations of TiO_2 nanoparticles and it is found that HA on the GB-3 surface (Fig. 7A(c))

was drastically reduced in contrast to other GB membranes (Fig. 7A(b and d)) and SB membranes (Fig. 7A(e–g)). The lower surface roughness of GB-3 denotes that this membrane could enhance the dislodgement of HA. The presence of the TiO_2-coated layer within the pores and surface of the uniformly coated layer of the GB-3 membrane had also assisted in the removal of HA by the photocatalysis of TiO_2 which consequently resulted in a greater flux and rejection rate (Fig. 7B(b), C, Table 2).

However, the accumulation of TiO_2 on the SB membrane surface not only creates high surface roughness, but also reduces the effective area of TiO_2 particles. It also lowers the membranes ability to reject HA (Fig. 7B(c)). Moreover, this effect also increases the deposition of HA on membrane surfaces that cannot be photocatalyzed by TiO_2. It will also reduce the rejection flux and rate during filtration (Fig. 7C, Table 2). The performance results proved that a TiO_2-coated layer on a GB-3 membrane surface has a dual function: antifouling and self-cleaning. This is similar to the previous study that added TiO_2 directly during the preparation of polysulfone/TiO_2 ultrafiltration membranes for HA removal [20].

Conclusions

In this study, porous photocatalytic ceramic membranes was successfully prepared using a phase inversion method via different dip-coating routes and characterized. By varying the concentrations of the coating medium for both dip-coating routes, different trends in the characteristics, properties and performance of membranes were obtained and measured. The significant conclusions of this study are highlighted as follows:

1. The uniform porous structure of GB-coated membranes proves that the ability of TiO_2 to penetrate deeper inside the main structure of a porous membrane (compared to the agglomeration effect of the TiO_2 layer when applied to a SB membrane surface) has created a rougher and non-uniform porous surface layer. Thus, penetration of TiO_2 nanoparticles inside GB membranes lowers the surface roughness, while accumulation of TiO_2 on the tighter structure of SB membrane surfaces increased the surface roughness.

2. The better response toward fouling of GB membranes increased the normalized flux ratio. This was attributed to a better coating of TiO_2 nanoparticles with a homogenous structure and a reduced agglomeration effect compared to that of SB membranes.

3. The uniform coating with lower surface roughness and a homogenous porous coating structure on GB-3 membranes improved the permeation of PWF and the rejection rate. The increasing TiO_2 nanoparticle filling effect on the GB-3 membranes produced optimum physical properties with the lowest diameter and thickness shrinkage, lower weight loss, lower porosity, lower mean pore radius, lower water absorption, as well as the highest density.

4. The ability of TiO_2 nanoparticles to self-clean as observed on GB-3 membrane surfaces is proven by the highly efficient removal of HA from the surface and a greater permeate flux and rejection rate after exposure to UV light. This revealed that uniform coating and the lowest possible surface roughness of the coating layer are very important to ensure that TiO_2 nanoparticles can work efficiently as a self-cleaning agent.

References

[1] Srikanth B, Goutham R, Narayan RB, Ramprasath A, Gopinath K, Sankaranarayanan A (2017) Recent advancements in supporting materials for immobilised photocatalytic applications in waste water treatment. J Environ Manage 200:60–78

[2] Hubadillah SK, Othman MHD, Harun Z, Ismail A, Rahman MA, Jaafar J, Jamil SM, Mohtor NH (2017) Superhydrophilic, low cost kaolin-based hollow fibre membranes for efficient oily-wastewater separation. Mater Lett 191:119–122

[3] Zangeneh H, Zinatizadeh A, Habibi M, Akia M, Isa MH (2015) Photocatalytic oxidation of organic dyes and pollutants in wastewater using different modified titanium dioxides: a comparative review. J Ind Eng Chem 26:1–36

[4] Nair AK, JagadeeshBabu PE (2017) TiO_2 nanosheet-graphene oxide based photocatalytic hierarchical membrane for water purification. Surf Coat Technol 320(Supplement C):259–262. https://doi.org/10.1016/j.surfcoat.2017.01.022

[5] Zhang Q, Wang H, Fan X, Lv F, Chen S, Quan X (2016) Fabrication of TiO_2 nanofiber membranes by a simple dip-coating technique for water treatment. Surf Coat Technol 298:45–52

[6] Abdullah HZ, Taib H, Sorrell CC (2007) Coating methods for self-cleaning thick films of titania. Adv Appl Ceram 106(1–2):105–112

[7] Abdullah H, Taib H, Sorrell C (2007) Coating methods for self-cleaning thick films of titania. Adv Appl Ceram 106(1–2):105–112

[8] Syafei AD, Lin C-F, Wu C-H (2008) Removal of natural organic matter by ultrafiltration with TiO_2-coated membrane under UV irradiation. J Colloid Interface Sci 323(1):112–119

[9] Yunos MZ, Harun Z, Basri H, Ismail AF (2012) Effects of water as non-solvent additive on performance of polysulfone ultrafiltration membrane. In: Advanced Materials Research. Trans Tech Publ, pp 46–50

[10] Harun Z, Shohur MF, Yunos MZ, Jamalludin MR, Ismail AF (2013) The effect of crystalline rice husk silica on polysulfone membrane for wastewater treatment. In: Applied Mechanics and Materials. Trans Tech Publ, pp 798–801

[11] Jamalludin MR, Harun Z, Basri H, Yunos MZ, Shohur MF (2013) Performance studies of polysulfone-based membrane: effect of silica morphology. In: Applied Mechanics and Materials. Trans Tech Publ, pp 8–12

[12] Harun Z, Kamarudin NH, Taib HM (2013) Effect of rice husk on fired ceramic shell strength. In: Advanced Materials Research. Trans Tech Publ, pp 732-737

[13] Harun Z, Kamarudin NH, Ibrahim M, Idris MI, Ahmad S (2015) Reinforced green ceramic shell mould for investment casting process. In: Advanced Materials Research. Trans Tech Publ, pp 415–419

[14] Oun A, Tahri N, Mahouche-Chergui S, Carbonnier B, Majumdar S, Sarkar S, Sahoo GC, Ben Amar R (2017) Tubular ultrafiltration ceramic membrane based on titania nanoparticles immobilized on macroporous clay-alumina support: elaboration, characterization and application to dye removal. Sep Purif Technol 188:126–133. https://doi.org/10.1016/j.seppur.2017.07.005

[15] Li K (2007) Ceramic membranes for separation and reaction. Wiley, New York

[16] Li X, Sotto A, Li J, Van der Bruggen B (2017) Progress and perspectives for synthesis of sustainable antifouling composite membranes containing in situ generated nanoparticles. J Membrane Sci 524:502–528

[17] Hristov P, Yoleva A, Djambazov S, Chukovska I, Dimitrov D (2012) Preparation and characterization of porous ceramic membranes for micro-filtration from natural zeolite. J Univ Chem Technol Metall 47(4):476–480

[18] Razmjou A, Resosudarmo A, Holmes RL, Li H, Mansouri J, Chen V (2012) The effect of modified TiO 2 nanoparticles on the polyethersulfone ultrafiltration hollow fiber membranes. Desalination 287:271–280

[19] Katsoufidou K, Yiantsios SG, Karabelas AJ (2005) A study of ultrafiltration membrane fouling by humic acids and flux recovery by backwashing: experiments and modeling. J Membrane Sci 266(1):40–50. https://doi.org/10.1016/j.memsci.2005.05.009

[20] Hamid NAA, Ismail AF, Matsuura T, Zularisam AW, Lau WJ, Yuliwati E, Abdullah MS (2011) Morphological and separation performance study of polysulfone/titanium dioxide (PSF/TiO$_2$) ultrafiltration membranes for humic acid removal. Desalination 273(1):85–92. https://doi.org/10.1016/j.desal.2010.12.052

[21] Stevenson FJ (1994) Humus chemistry: genesis, composition, reactions. Wiley, New York

[22] Xue G, Liu H, Chen Q, Hills C, Tyrer M, Innocent F (2011) Synergy between surface adsorption and photocatalysis during degradation of humic acid on TiO 2/activated carbon composites. J Hazard Mater 186(1):765–772

[23] Birben NC, Uyguner-Demirel CS, Kavurmaci SS, Gürkan YY, Turkten N, Cinar Z, Bekbolet M (2017) Application of Fe-doped TiO$_2$ specimens for the solar photocatalytic degradation of humic acid. Catal Today 281:78–84

[24] Leong S, Razmjou A, Wang K, Hapgood K, Zhang X, Wang H (2014) TiO$_2$ based photocatalytic membranes: a review. J Membrane Sci 472:167–184

[25] Fukushima M, Tatsumi K, Nagao S (2001) Degradation characteristics of humic acid during photo-Fenton processes. Environ Sci Technol 35(18):3683–3690

[26] Xue G, Liu H, Chen Q, Hills C, Tyrer M, Innocent F (2011) Synergy between surface adsorption and photocatalysis during degradation of humic acid on TiO 2/activated carbon composites. J Hazard Mater 186(1):765–772

[27] Park H, Park Y, Kim W, Choi W (2013) Surface modification of TiO$_2$ photocatalyst for environmental applications. J Photochem Photobiol C Photochem Rev 15:1–20